



Insight into structural rearrangements and interdomain interactions related to electron transfer between flavin mononucleotide and heme in nitric oxide synthase: A molecular dynamics study



Yinghong Sheng ^{a,*}, Linghao Zhong ^b, Dahai Guo ^c, Gavin Lau ^a, Changjian Feng ^{d,*}

^a Department of Chemistry & Physics, College of Arts & Sciences, Florida Gulf Coast University, 10501 FGCU Blvd. S., Fort Myers, FL 33965, USA

^b Pennsylvania State University at Mont Alto, 1 Campus Drive, Mont Alto, PA 17237, USA

^c Department of Bioengineering and Software Engineering, U.A. Whitaker College of Engineering, Florida Gulf Coast University, 10501 FGCU Blvd. S., Fort Myers, FL 33965, USA

^d Department of Pharmaceutical Sciences, College of Pharmacy, University of New Mexico, Albuquerque, NM 87131, USA

ARTICLE INFO

Article history:

Received 25 April 2015

Received in revised form 29 June 2015

Accepted 5 August 2015

Available online 7 August 2015

Keywords:

Molecular dynamics

Nitric oxide synthase

Electron transfer

Heme

Calmodulin

ABSTRACT

Calmodulin (CaM) binding to nitric oxide synthase (NOS) enables a conformational change, in which the FMN domain shuttles between the FAD and heme domains to deliver electrons to the active site heme center. A clear understanding of this large conformational change is critical, since this step is the rate-limiting in NOS catalysis. Herein molecular dynamics simulations were conducted on a model of an oxygenase/FMN (oxyFMN) construct of human inducible NOS (iNOS). This is to investigate the structural rearrangements and the domain interactions related to the FMN–heme interdomain electron transfer (IET). We carried out simulations on the iNOS oxyFMN·CaM complex models in [Fe(III)][FMNH[–]] and [Fe(II)][FMNH[·]] oxidation states, the pre- and post-IET states. The comparison of the dynamics and conformations of the iNOS construct at the two oxidation states has allowed us to identify key factors related to facilitating the FMN–heme IET process. The computational results demonstrated, for the first time, that the conformational change is redox-dependent. Predictions of the key interacting sites in optimal interdomain FMN/heme docking are well supported by experimental data in the literature. An intra-subunit pivot region is predicted to modulate the FMN domain motion and correlate with existence of a bottleneck in the conformational sampling that leads to the electron transfer-competent state. Interactions of the residues identified in this work are proposed to ensure that the FMN domain moves with appropriate degrees of freedom and docks to proper positions at the heme domain, resulting in efficient IET and nitric oxide production.

© 2015 Elsevier Inc. All rights reserved.

1. Introduction

Nitric oxide (NO) is a key signaling molecule for vasodilation and neurotransmission at low concentrations and a defensive cytotoxin at higher concentrations [1,2]. Nitric oxide synthase (NOS) is the enzyme responsible for biosynthesis of NO from L-arginine. NO's availability is tightly regulated at the synthesis level by NOS. Deviant NO production by NOS is a major contributor to the pathology of often fatal diseases that currently lack effective treatments, including stroke [3]. To date, clinical NOS modulators still remain elusive. Before logically designing an effective therapeutic strategy by targeting NOS/NO, one must understand the mechanism of NOS regulation at the molecular level. Yet, there is still much unknown about the mechanism of tight regulation of NO production by NOS. It is thus of current interest to investigate regulation mechanisms of the NOS enzymes.

Mammalian NOS enzyme catalyzes the 5-electron oxidation of L-arginine (L-Arg) to NO and citrulline, utilizing NADPH and O₂ as co-substrates [1]. NOS is a redox enzyme consisting of multiple relatively rigid domains that are connected by flexible linkers. Each subunit of the NOS homo-dimer has two domains joined by a calmodulin (CaM) binding linker: a C-terminal electron-supplying reductase domain, which consists of smaller (sub)domains with binding sites for NADPH (the electron source), flavin adenine dinucleotide (FAD), and flavin mononucleotide (FMN), and an N-terminal catalytic oxygenase domain with heme, tetrahydrobiopterin (H₄B), and arginine substrate binding sites forming the catalytic center for NO production (the terms 'oxygenase domain' and 'heme domain' are interchangeable). NOS's activity depends in equal measure on the reactions at the heme active site and on the overall dynamic structural rearrangements that enable the timely delivery of electrons to the active site (see below).

Three NOS isoforms, iNOS, eNOS and nNOS (inducible, endothelial, and neuronal NOS), achieve their biological functions by tight control of interdomain electron transfer (IET) process through interdomain interactions [4,5]. In particular, inter-subunit FMN–heme IET (Eq. (1)) is

* Corresponding authors.

E-mail addresses: ysheng@fgcu.edu (Y. Sheng), cfeng@umn.edu (C. Feng).

the essential step in coupling electron transfer in the reductase domain with NO synthesis in the heme domain by delivery of electrons required for O₂ activation at the catalytic heme site [6].



The protonation state of the NOS flavin hydroquinone is not known yet, and FMN_{hq} is used to represent FMN hydroquinone in Eq. (1). The FMN–heme IET process is proposed to involve large scale motions of the FMN domain (Fig. 1) [5]. Starting from the NADPH–FAD/FMN state (i.e., electron-accepting input state), the FMN molecule receives an electron from the FAD center, and is reduced to FMN_{hq}. The FMN domain then moves away from the NADPH–FAD domain and migrates to the oxygenase domain (forming the output state) so that the FMN_{hq} can deliver an electron to the heme center, where Fe(III) is reduced to Fe(II) and the FMN center is converted to its semiquinone form FMNH^{*}. Subsequently, the FMN domain moves away from the heme domain toward back to the NADPH–FAD domain (to shuttle another NADPH-derived electron). This FMN domain tethered shuttle model (Fig. 1) has been supported by recent kinetics [7–16], thermodynamic [17] and spectroscopic [18,19] results. Emerging evidence indicates that CaM activates NO synthesis in eNOS and nNOS by allowing the conformational change, and that CaM is also required for proper alignment of the FMN and heme domains [4,5]. However, the control mechanism underlying the large movement of the FMN domain between the NADPH–FAD and heme domains remain unclear. The precise role of CaM regulating this conformational change, especially how CaM interacts with the heme domains and constrains the motions of the FMN domain, is poorly understood [20].

A full-length NOS structure will help understand the NOS regulation mechanism. Unfortunately, the mobility of the NOS domains makes crystallization of the full-length enzyme very challenging, thus the structure of full-length NOS has not been obtained. Even if such crystal structures were available, the molecular mechanisms that promote function may still remain elusive, since NOS is a highly dynamic protein existing in a broad range of interconverting conformations [21,22]. The crystals can only stabilize some specific structural sub-states that define the functional state of the protein. Thus, X-ray crystallography alone will not solve the NOS structural problems and may only shed light on some of the static structural details without addressing the dynamics aspects.

Electron microscopy (EM) is a useful method for determining the structures of large proteins and protein complexes. In the last two years, four cryo-EM studies of the three full-length NOS isoforms were published [23–26], giving substantial insight into the molecular architecture of NOSs. This also attests an urgent need of elucidating conformational changes required for efficient electron transfer. However,

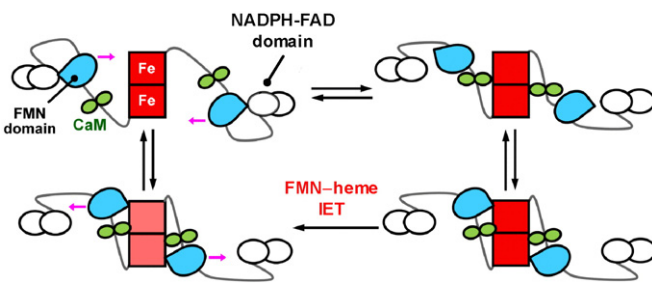


Fig. 1. The FMN domain tethered shuttle model (with the tethers corresponding to the interdomain FMN–heme and FAD–FMN connectors). The FMN domain (cyan) shuttles between the NADPH–FAD domain (white) and the heme-containing oxygenase domain (red). CaM (green) binding to eNOS/nNOS unlocks the NADPH–FAD/FMN domain interacting state (i.e., input state), thereby enabling the FMN domain to shuttle between the FAD and heme domains. The input state and FMN–heme domain interacting state (i.e., output state) are relatively well defined, while free FMN domain conformations also exist in between these two docked states.

structures determined by cryo-EM are of low resolution, and the classification of the conformational states in these works is categorized according to the perceived overall shapes of the entire dimer, but not the precise relative arrangement of the specific structural parts of the protein. At low resolutions (23 Å [25] and 60–74 Å [23]), cryo-EM cannot provide explicit information on the interactions between the FMN and heme domains. Moreover, the authors used negative-stain EM methods, which involved fixing the protein sample on a carbon-coated surface and treating it with a high-contrast heavy metal stain. While this is a powerful approach for observing protein complexes, in certain cases the grid surface can distort the sample and lead to a debatable asymmetry [23].

Magnetic resonance and fluorescence-based approaches represent a powerful complement to traditional structural biology methods and are now increasingly used to probe the NOS structure and function. The size of the NOS enzymes (~120–160 kDa per subunit) prevents application of NMR spectroscopy with methods available to date, although ¹³C- and ¹⁵N-labeled CaM proteins were recently used in the NMR studies of structure and dynamics of CaM bound to peptides corresponding to the CaM-binding linker in the NOS proteins [27,28]. Fluorescence resonance energy transfer approach can provide distance data, but there are known complexities when using the intrinsic fluorophores FMN and FAD since their fluorescence quantum yields depend on solvent accessibility and redox state. Tagging the protein domains with donor and acceptor fluorophores may be a better approach, but it needs to be tested if the bulky tags interfere with the NOS activity.

A clear understanding of the large NOS conformational change is critical, since this step is the rate-limiting in NO production [23]. While experimental approaches still face tremendous challenges at this moment, computational simulation can provide valuable information on the dynamics of enzyme structures, key residue–residue interaction evolution, and hence facilitate the understanding of the roles of inter-domain interactions and protein dynamics in NOS regulation. Up to date, no computational simulation has been reported to elucidate the domain motions in NOS. The time scale for the interconverting between input and output states has not been experimentally measured, but should be at milliseconds to seconds range since the rates of similar FMN domain binding of and release from the FAD domain are estimated to be around 10 s⁻¹ [29,30]. Such long time scale is beyond current computational simulation capacity.

We thus focused on studying the dynamics of the NOS output state using models of a CaM-bound bi-domain oxygenase/FMN (oxyFMN) construct. This construct is a minimal electron transfer complex designed to favor the interactions between the FMN and heme domains [31], and biochemical and kinetics studies demonstrated that it is a valid representation of the NOS output state for NO production [4,5]. In the present work, we have conducted molecular dynamics (MD) simulations on the two redox states before and after the IET process (Eq. (1)). Based on the initial docking model for a human iNOS oxyFMN construct, MD simulations were carried out to elucidate the structural rearrangements and the interactions between domains. Specifically, we examined role of redox states change (due to the IET) in the conformational changes. The comparison of the dynamics and structures of the NOS oxyFMN construct at the two oxidation states has allowed us to identify key factors related to facilitating the FMN–heme IET process. The predictions of key interacting sites are well supported by experimental data in the literature, and new sites have also been identified from the simulation. These computational results have provided new insight into the dynamic interactions in regulating the NOS electron transfer and function.

2. Methods

2.1. Initial structure construction

The initial docked structures of human iNOS oxyFMN·CaM construct were built using the crystal structures of human iNOS heme domain

(PDB code 1NSI) [32] and human iNOS FMN domain bound with CaM (PDB code 3HR4) [33] as the input files for ZDOCK [34,35]. Experimental studies showed that equivalent residues of Arg241 and Lys445 from the heme chain A [36–38], along with Glu546, Asp597, and Glu661 from the FMN domain [38,39], are important in the interdomain FMN/heme interactions. Therefore, we imposed the presence of these residues in the docking interface. The ZDOCK generated structures were then filtered by two criteria: (i) the N₅ atom of FMN and heme Fe distance should be around 19 Å, which is determined by pulsed EPR [40] (this distance is also necessary for an efficient electron transfer), and (ii) the distance between Gln502 (C terminus of the heme domain structure) and Arg511 (N terminus of the CaM bound FMN domain structure) should be less than 30 Å, the maximum length for 10 missing residues that connect these two ends. Only one ZDOCK model, satisfied both criteria, in which the distance between heme Fe atom and N₅ atom of FMN domain amounts to 20.6 Å and the distance between C_α atoms of Gln502 and Arg511 is 20.5 Å. The missing residues connecting the heme and FMN domains were then added to this model using Scigress Explorer Ultra 7.7 (Fujitsu) and further refined by energy minimization using NAMD [41] with CHARMM27 force field [42]. The constructed docked structure (Fig. 2) is overall superimposable to the docked structure reported by Marletta's group [43].

2.2. Parameterizations of the heme, FMN and H₄B cofactors

The iron ion switches between oxidized Fe(III) state and reduced Fe(II) state during the FMN–heme IET process (Eq. (1)). The heme iron has an axial cysteine ligand. To account for the coordinated cysteine residue on the heme atom partial charges, we carried out B3LYP optimizations at the DFT level with sextet and quintet multiplicities for heme [44]. The basis sets were a LACVP basis set, which includes the highest s, p, and d shells of iron (the outermost core orbitals for iron) and a 6-31G basis set for both the rest of the heme moiety and the cysteine (Cys200) ligand atoms. The Los Alamos effective core potential was applied on iron [45], along with matching basis sets. Modified charges were based on electrostatic potential (ESP) charges obtained from a solvent continuum calculation [46]. The atomic charges on α-, β- and meso-carbons as well as on the pyrrole nitrogens were adjusted to account for the different charge distributions. The force field parameters of ferric heme were obtained from previous works [47,48]. Similar to the work by Autenrieth et al. [48], we used the same bonded equilibrium values and force constants for both forms of the heme iron

(i.e., Fe(III) and Fe(II)), and differentiated them only with respect to partial atomic charges.

The FMN cofactor switches between 2-electron reduced hydroquinone state FMN_{hq} and 1-electron reduced semiquinone state FMNH[·] during the IET (Eq. (1)). The CHARMM force field parameters for FMN were adapted from the work of Freddolino et al. [49]. Standard CHARMM atom types were utilized, and charges were derived from QM calculations. All structures were optimized at the B3LYP/6-31G* level of theory, including the CPCM solvation model to better account for the charge distribution in solutions. Additional force field parameters were chosen in analogy to standard CHARMM parameters, or derived from the QM optimized geometries [46,50].

The similar parameterization procedure was applied to the H₄B cofactor. Briefly, the atomic charges of the atoms on the fused rings were obtained from the ESP charges at the B3LYP/6-31G* level of theory, and the charges for the other atoms were standard CHARMM27 atomic charges [42].

The topologies of ferrous heme, ferric heme, FMN semiquinone, FMN hydroquinone, and H₄B are included in the Supporting Information S1.

2.3. Molecular dynamics simulations

All MD simulations were carried out using NAMD [41] with a conjunction of CHARMM force field [42] and the cofactors' parameters we developed. The simulations were performed in a 144 × 108 × 125 Å³ TIP3 [51] water box, allowing a minimum of 15 Å water solvation shell for each protein atom. Counter ions (Na⁺ and Cl[−]) were added to bring the whole system to a charge-neutral state. Periodic boundary conditions were applied on the box throughout the simulations. The constructed system was first minimized for 5000 steps, with the protein core held fixed while water and ions were relaxed. Subsequently, the whole system was fully minimized to remove any internal constraints.

The minimized system was then heated from 0 to 310 K with a 10 K increment, followed by 20 ps of equilibration. Finally, 60 ns production trajectories were collected for this system in the canonical NVT ensemble, using a Verlet algorithm for the integration with a 2 fs step size. Nonbonding interactions were treated using a cutoff of 12.0 Å. Electrostatic interactions were calculated with the particle mesh Ewald summation. Multiple independent MD trajectories were collected for each system.

3. Results and discussion

In this work we investigated iNOS oxyFMN·CaM dynamics before and after the FMN–heme IET, the catalytically essential step in NOS catalysis [6]. Since the IET (Eq. (1)) involves different oxidization states of the Fe and FMN centers, both the [Fe(III)][FMN_{hq}] and [Fe(II)][FMNH[·]] states have been examined. The protonation state of FMN hydroquinone is not known yet. We thus conducted MD simulations on the [Fe(III)][FMN_{hq}] state containing either FMNH[−] or FMNH₂. Similar trajectory the Fe–N₅ (FMN) distance was obtained for both cases (Fig. S1 in Supporting Information). For the sake of clarity, we only discussed the FMNH[−] state (for the FMN hydroquinone form) in details in the following sections.

3.1. Structural and dynamic properties of the [Fe(III)][FMNH[−]] state before the FMN–heme IET

In the FMN–heme IET (Eq. (1)), the [Fe(III)][FMNH[−]] is defined as the pre-IET state. Starting from the initial model of the human iNOS oxyFMN·CaM (Fig. 2), a 60 ns MD simulation on the protein at the pre-IET state was performed. Trajectory *a* in Fig. 3 shows the corresponding backbone root-mean-square deviations (rmsd) from the initial structure. Note that during the 60 ns simulations the rmsd reaches stable values after ~10 ns, and minor fluctuations take place afterward. We repeated the MD simulation by collecting another 60-ns trajectory

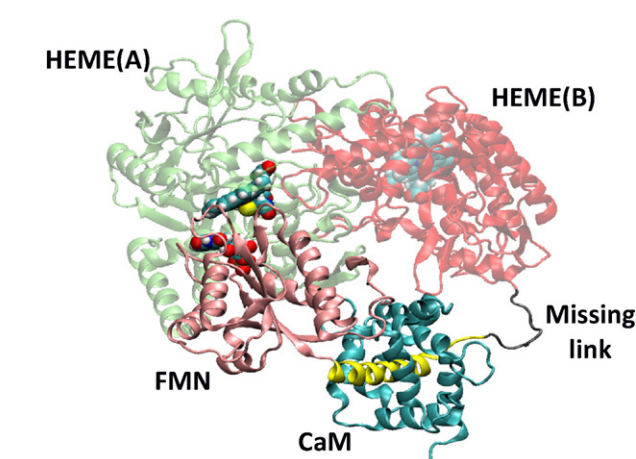


Fig. 2. Initial docked structure of the FMN domain (pink) and the dimeric heme domains A and B (green and red) along with CaM-binding motif (yellow) bound with CaM (cyan). The missing linker residues (in black) were added by using Scigress and further refined by energy minimization using NAMD software. Note that the FMN domain in subunit B docks to the heme domain in subunit A.

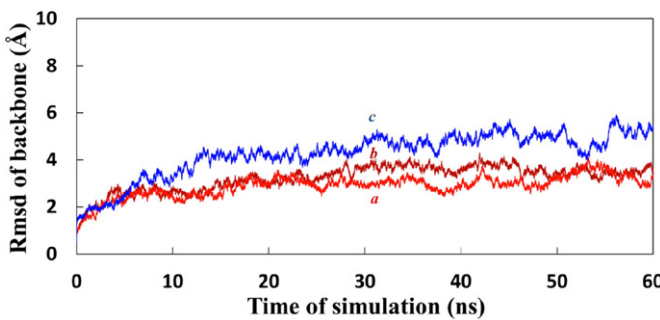


Fig. 3. Root-mean-square deviation (rmsd) for the backbone of human iNOS oxyFMN·CaM at the pre-IET [Fe(III)][FMNH⁺] state (a, b) and the post-IET [Fe(II)][FMNH⁺] state (c).

b. Both trajectories (a and b in Fig. 3) gave similar results. Therefore, such conformational changes in the MD simulations are not random.

We next examined if the interdomain FMN/heme alignment obtained from the simulations would facilitate an effective FMN–heme IET. First the distance between the heme and FMN centers were assessed since distance between redox centers is critical for controlling electron transfer in proteins [52]. Fig. 4 shows the two trajectories of the Fe···N₅ (FMN) distance in the two 60 ns MD simulations (red and green traces). After the rapid initial stabilization (0–10 ns), the Fe···N₅ (FMN) distance stays at ~22 Å, which allows efficient IET.

Three typical IET-competent conformations (Fig. 5) were identified from the simulations. The major structural difference among the conformations is the orientation of the FMN molecule related to the heme center. These conformations represent different feasible electron transfer pathways between the heme and FMN centers. The electrostatic potential surfaces of the heme and FMN molecules in the three conformations were computed at the B3LYP/6-31G(d) level, and no direct overlap between their electron densities was noticed (image not shown). This indicates that an electron is not preferably transferred directly from the FMN to the heme molecule. Instead, residues located between the heme and FMN centers participate in the long-range IET. Fig. 5 shows the plausible IET pathways in these conformations.

In the first conformation (Fig. 5a), the heme A domain residue Trp372 is in close contact with the heme cofactor (the distance between heme Fe and Trp372 C_β atom amounts to ~10 Å), while the distance between Trp372 C_β and FMN N₅ is slightly longer, being about 14 Å. The B3LYP computed molecular electrostatic potential (Fig. 5b) showed that Trp372 does not directly overlap with the FMN molecule; instead the FMN domain residue Phe593 was found to serve as an electron transfer bridge. In this case, electron transfer would proceed through FMN, Phe593, Trp372, and heme (Fig. 5a). Such a process involves three through-space jumps: the first from the isoalloxazine ring of FMN to the phenyl ring of Phe593, the second from Phe593 to the indole

ring of Trp372, and then the third from Trp372 to the vinyl group of the heme center.

Fig. 5c and e show the other two conformations where FMN is located at the Cys200 side of the heme porphyrin ring plane. In the conformation shown in Fig. 5c, the distances from heme A domain residue Trp372 C_β atom to heme Fe and to FMN N₅ atoms amount to 10 and 12 Å, respectively. The B3LYP computed molecular electrostatic potential (Fig. 5d) shows significant electron density overlap between the indole ring of Trp372 and the isoalloxazine ring of the FMN molecule. Thus in this conformation an electron can be transferred from FMN to the heme center through the heme A residue Trp372. On the other hand, in the third conformation shown in Fig. 5e, the distances from heme A domain residue Trp372 C_β atom to heme Fe and to FMN N₅ atoms are 10 and 14 Å, respectively. Apparently, efficient electron transfer from FMN to Trp372 is hampered at such a distance. A FMN domain residue Tyr631 is found lying in between. The electrostatic potential surface (Fig. 5f) shows that phenyl ring of Tyr631 overlaps with the indole ring of the heme A domain residue Trp372. Therefore the FMN domain residue Tyr631 is also involved in mediating the FMN–heme IET in the third conformation.

The above conformations thus represent three plausible electron transfer pathways between the heme and FMN centers. The electron transfer proceeds through two or three through-space jumps, first from the isoalloxazine ring of FMN to either phenyl ring of Phe593 or Tyr631 and then to the indole ring of Trp372, or directly to the indole ring of Trp372, and eventually to the vinyl group of heme center. In all the three conformations the Trp372 residue is involved in the electron transfer. Indeed, experimental results [43] showed a significant decrease in the rate of heme reduction in the W → A mutant, consistent with its predicted role in conducting electrons to the heme. Our MD simulation and electrostatic potential surface results also indicate that the FMN domain residues Phe593 and Tyr631 are involved in mediating the IET. Their roles in the IET need to be validated by mutational and biochemical experiments.

The above results prompted us to further identify residues at the interacting interface between the FMN and the heme domains, which preserve the FMN center well poised with the heme center in the IET-competent conformations. Since the two MD simulations we collected show similar results (trajectories a or b in Fig. 3), we only described in detail the residue–residue interactions in the first simulation (trajectory a in Fig. 3).

The residue–residue interactions in the oxyFMN·CaM complex during the 60 ns period were analyzed and are summarized in Table S1 of Supporting Information. The residue–residue interactions can be categorized into three groups: 1) inter-subunit interactions between the heme A and FMN domains; 2) intra-subunit interactions between the heme B and FMN domains; and 3) inter-protein interactions between the NOS heme domains and CaM. These three groups of interacting residues are described below, and selected interacting pairs are shown in Figs. 6–9.

Group 1 – Inter-subunit interactions between the FMN domain and heme A domain (Fig. 6) are found to facilitate the docking. Electrostatic interacting pairs comprise the majority of the interactions. Specifically, heme A domain residue Lys445 forms a salt bridge with FMN domain residue Glu551, and the guanidinium group of Arg241 in heme A domain maintains a salt bridge with the carboxylate group of Glu546 in the FMN domain. Additionally, heme A domain residues Gln427 and Asn430 form strong hydrogen bonds with backbone oxygen atom of the FMN domain residue Tyr631. The roles of the predicted ionic interacting residues in the FMN–heme IET are supported by experimental findings: the equivalent residue pairs in rat nNOS are required to form an interdomain interface for efficient IET [36–38]. Additionally, Glu546, a conserved charged surface residue of the FMN domain in human iNOS, has been shown to participate in the interdomain FMN–heme interactions [53,54], and the notable slower IET in the E546N mutant is caused by a lower population of the IET-active conformation [55].

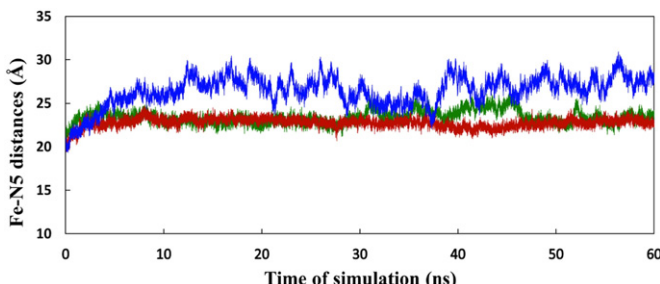


Fig. 4. The Fe···N₅ (FMN) distance in the pre- (red, green) and post-IET (blue) states during the MD simulations.

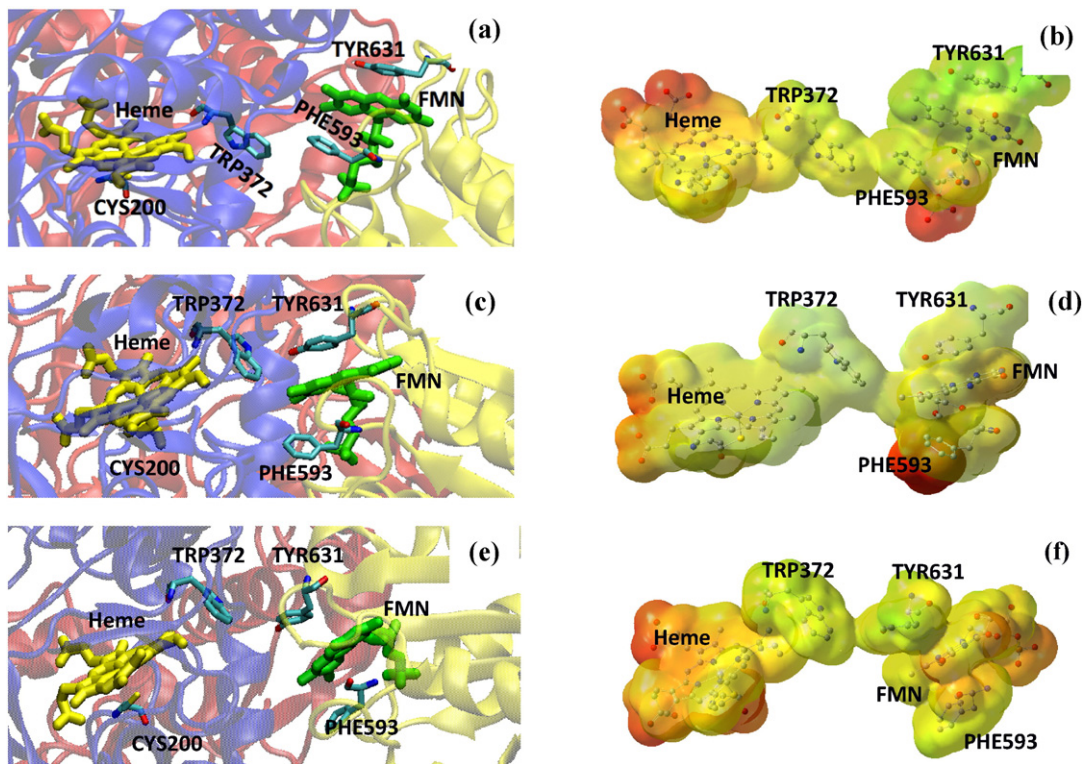


Fig. 5. Typical IET-competent NOS conformations with the FMN and heme molecules shown in green and yellow Licorice modes, respectively. In the three conformations the FMN approaches different sides of the heme porphyrin ring. (a) *Conformation 1*: IET presumably takes place through FMN → Phe593 → Trp372 → heme center. (c) *Conformation 2*: IET takes place through FMN → Trp372 → heme center. (e) *Conformation 3*: IET takes place through FMN → Tyr631 → Trp372 → heme center. (b, d, f) The B3LYP computed molecular electrostatic potentials for the conformations 1, 2, and 3, respectively.

Group 2 – Throughout the simulations, the heme B domain loop consisting of residues His404, Lys405, and Leu406 is in close contact with the FMN domain loop consisting of residues Glu661–Gln666 (Fig. 6). Specifically, residue His404 (heme B) forms a strong salt bridge with Gln666 (FMN), and a His404 (heme B)–Gln666 (FMN) hydrogen

bond also exists. Leu406 (heme B) interacts strongly with Gln665 (FMN) through a hydrogen bond as well. In addition, Lys405 (heme B) forms a salt bridge with Glu661 (FMN). These intra-subunit interactions appear to effectively maintain the IET-favorable orientation of the FMN domain with respect to the heme domain (see Fig. 5 above).

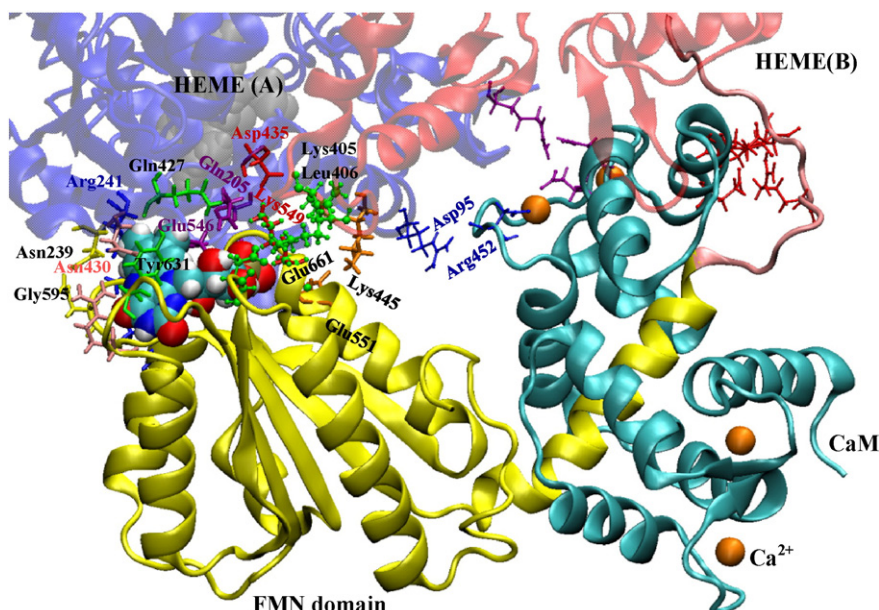


Fig. 6. Selected key residues in the interfaces between heme, FMN and CaM domains in the pre-IET state. Heme A domain, heme B domain and CaM are represented as blue, red, and cyan ribbons, respectively. The FMN domain is shown as yellow ribbon. Refer to Figs. 7–8 for the detail information on the residue–residue interactions on each interface.

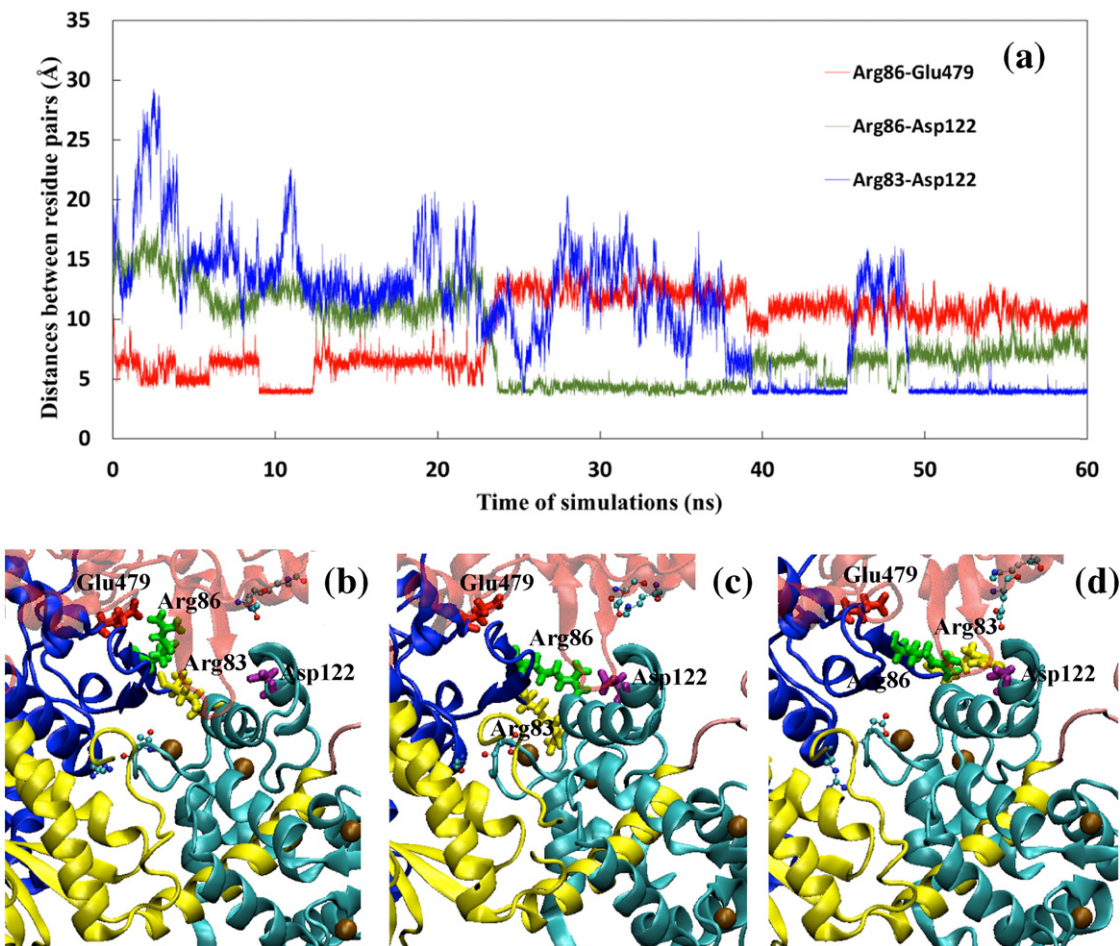


Fig. 7. (a) During the 60 ns simulation course of the pre-IET state, the distances between heme A domain residues Arg86 guanidinium carbon atom (CZ) and Glu479 carboxylate group carbon (CD) atom (red trajectory), between heme A domain residue Arg86 CZ atom and CaM residue Asp122 carboxylate carbon (CG) atom (green trajectory), and between heme A residue Arg83 CZ atom and CaM residue Asp122 CG atom (blue trajectory). (b) Initially, heme A domain residue Arg86 (green Licorice mode) forms a salt bridge with Glu479 (red Licorice mode) of the same domain. (c) At ~22 ns, the Arg86 residue (green Licorice mode) forms a salt bridge with CaM residue Asp122 (purple Licorice mode). (d) At ~40 ns, heme A domain residue Arg83 (yellow Licorice mode) forms a salt bridge with CaM residue Asp122 (purple Licorice mode). Heme A domain, heme B domain and CaM are represented as blue, red, and cyan ribbons, respectively. The FMN domain is shown as yellow ribbon.

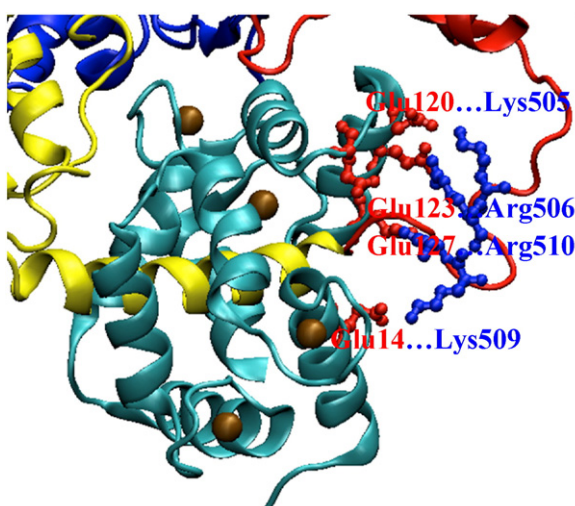


Fig. 8. Salt bridges between CaM (cyan) and the linker region of the heme B domain (red) in the pre-IET state. The negatively charged CaM residues (Glu14, Glu120, Glu123, Glu127) are labeled in red. The positively charged linker residues Lys505, Arg506, Arg510, and Lys509 are labeled in blue. The FMN domain is in yellow.

Moreover, they are also likely involved in the large movement of the FMN domain after the IET (see below).

Group 3 – Inter-protein interactions between the NOS heme domains and CaM include a Gln97 (heme A)–Gln135 (CaM) salt bridge and a Gln97 (heme A)–Asn97 (CaM) hydrogen bond. Another hydrogen bond is found between Asp95 (CaM) and the backbone oxygen atom of Arg452 (heme A).

It is worthy of note the dynamic changes in the interactions between CaM and the N-terminus of the heme A domain. In the initial constructed conformation, the N-terminal Arg86 (heme A) is far away from CaM (Fig. 7b), and interacts with Glu479 (heme A) via an intra-domain salt bridge (red trajectory in Fig. 7a). With the progress of MD simulation, Arg86 gradually swings over toward CaM, and forms a stable salt bridge at ~22 ns with Asp122 in the CaM domain (green trajectory in Fig. 7a). This new interaction effectively pulls CaM closer to the heme A domain (Fig. 7c). After a while, this salt bridge is substituted by another salt bridge between Arg83 (heme A) and Asp122 (CaM) (see Fig. 7d and blue trajectory in Fig. 7a). Despite the competition between Arg86 and Arg83, the heme A domain is constantly bound to the CaM via a strong and stable salt bridge. In other words, CaM docking to the heme domain is well maintained in the IET-compatible conformations throughout the simulation period. Recent hydrogen deuterium exchange mass spectrometry and kinetics studies demonstrated the importance of CaM

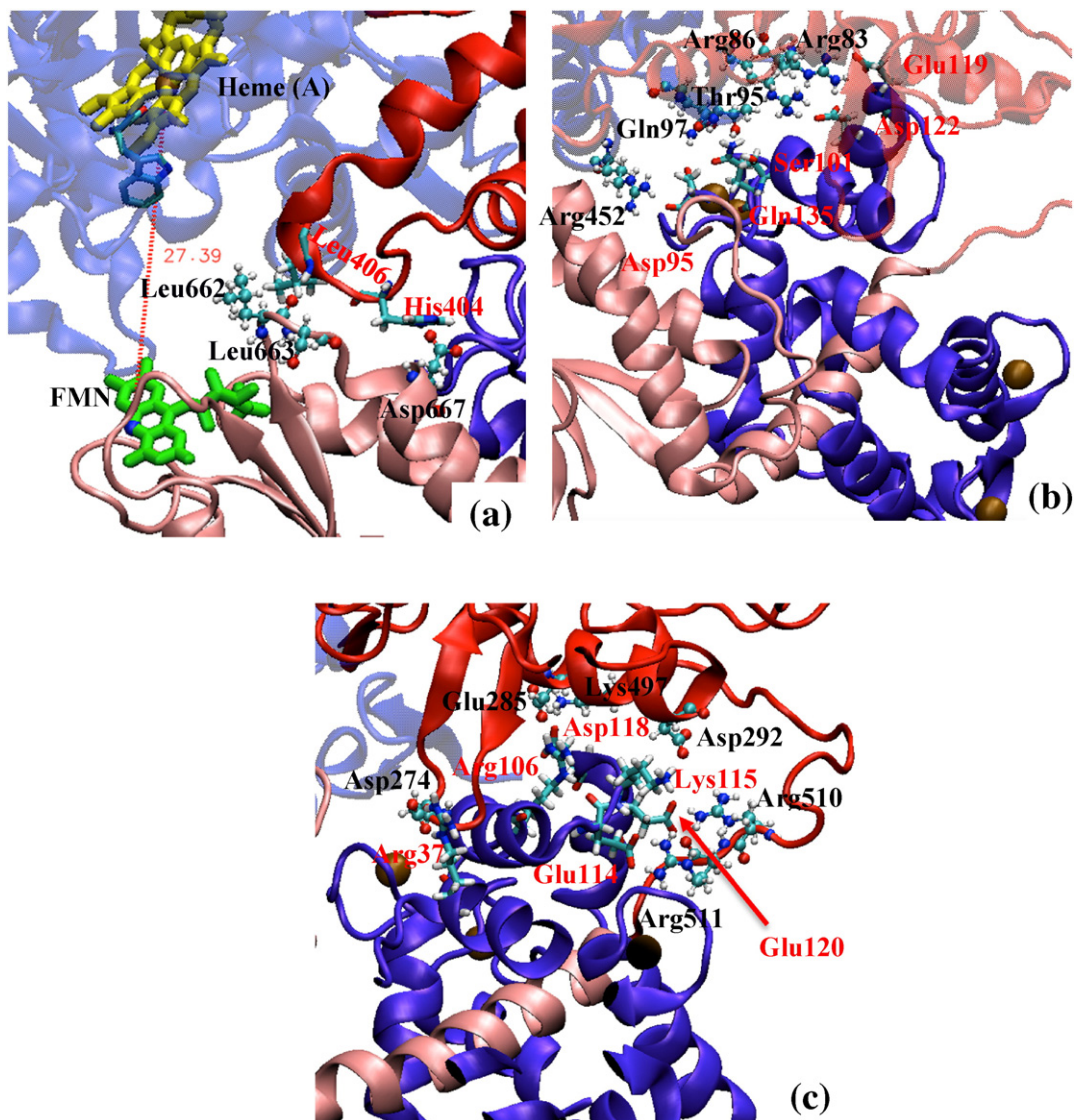


Fig. 9. Inter-domain interactions in the post-IET state. Heme A, heme B, CaM and FMN domains are represented in pale blue, red, pink and violet ribbons, respectively. (a) The Fe···N₅ (FMN) distance at this snapshot amounts to 27.4 Å. (b) The interactions between the heme A and CaM domains. (c) The interactions between the heme B and CaM domains.

docking to the heme domain for the electron transfer in murine iNOS [43]. Their experimental results showed that the CaM surface encompassing Arg106, Lys115, and Asp118 interacts with the murine iNOS heme domain residues Arg80 and Glu279 (equivalent to human iNOS residues Arg86 and Glu285), where complementary electrostatic interactions facilitate the interdomain CaM/heme alignment. This is generally in agreement with our simulation results for human iNOS (see also Table S1). It is also interesting to note that two other CaM residues affecting the kinetics, Lys21 and Lys30, don't make any obvious charge pairing contacts with the heme domain in their docking model [43], suggesting that the heme domain and CaM undergo some conformational change upon CaM-NOS(heme) binding, which would bring these two residues into closer contact with the heme domain in other conformations. In other words, when it is near the NOS heme domain, CaM samples the heme domain surface and docks through distinct interfaces.

The linker between the heme B and FMN domains was reconstructed from its amino acid sequence. Being rich in positively charged residues, this linker naturally forms multiple salt bridges with five CaM glutamic acid residues (Fig. 8).

3.2. Structural and conformational changes of the protein state [Fe(II)][FMNH⁺] after the IET

The preceding sections are on the pre-IET state, i.e., [Fe(III)][FMNH[−]]. After the IET, Fe(III) is reduced to Fe(II), and the FMN cofactor is converted to FMNH⁺. A 60 ns MD simulation of the protein conformations at the resulting state of [Fe(II)][FMNH⁺] (referred as the post-IET state hereafter) was performed. Another two 30 ns MD simulations were also carried out and obtained similar results. Therefore, the discussion below focused on the 60 ns MD simulation results. Blue trajectory in Fig. 3c shows the backbone rmsd of this post-IET state during the 60 ns MD simulation. It is obvious that, after the IET has occurred, the protein structure changes more from its initial structure, compared to that of the pre-IET state (blue vs. red trajectories, Fig. 3). Moreover, the final Fe···N₅ (FMN) distance became much larger than that of pre-IET (blue vs. other trajectories, Fig. 4). A snapshot of the FMN and heme interface at 60 ns is illustrated in Fig. 9a. The Fe···N₅ (FMN) distance has increased to 27.4 Å, indicating the departure of the FMN domain after the IET. To further verify whether the redox state influences the docking of the

FMN domain onto the heme domain, we performed another 45 ns MD simulation using a post-IET conformation in which the $\text{Fe}\cdots\text{N}_5$ (FMN) distance amounts to 30.5 Å, but with the oxidation state $[\text{Fe}(\text{II})]\text{[FMNH}^-]$ changed to $[\text{Fe}(\text{III})]\text{[FMNH}^-]$ (i.e., a pre-IET state possessing a post-IET distance). While starting with an post-IET conformation, the FMN domain readily recovers its docking with heme A domain (Fig. S2): the $\text{Fe}\cdots\text{N}_5$ (FMN) distance quickly reverts back to around 22 Å. This showed that the docked FMN/heme conformation can be easily realized in the pre-IET redox state, which is independent of the initial structure. These MD simulations together clearly demonstrated that the FMN domain departure after the IET is primarily induced by oxidation state change.

Importantly, the large fluctuation in the distance between the heme and FMN domains from the MD simulation (blue trajectory in Fig. 4) revealed a highly dynamic nature of the NOS protein in its post-IET state. After the overall protein structure stabilizes at ~10 ns, the $\text{Fe}\cdots\text{N}_5$ (FMN) distance notably fluctuates between 26 and 31 Å. Statistically, the majority of the conformations in the simulation have a $\text{Fe}\cdots\text{N}_5$ (FMN) distance > 27 Å, while some reach 31 Å. Only 16% of the conformations have a distance < 25 Å. Therefore, after the IET the FMN domain becomes quite mobile, allowing the FMN domain to shuttle between the FAD and heme domains to transfer electrons across the protein.

The key inter-domain interactions after the IET are illustrated in Fig. 9b and c. Note that the FMN domain has begun to swing away from the heme A domain after the IET (see Fig. 10). All the inter-subunit interactions between the heme A and FMN domains found in the pre-IET state thus no longer exist (Fig. 10a). On the other hand, during the 60 ns simulation, certain intra-subunit interactions between the heme B and FMN domains are well maintained. Heme B residue Leu406 is always hooked with the FMN domain residues Leu662 and Leu663 through hydrogen bonds, and His404 (heme B) is in close contact with Asp667 (FMN). Comparing with the 'Group 2' interacting residues in the pre-IET state (heme B domain residues His404, Lys405, and Leu406 and FMN domain residues Glu661, Leu662, Gln665, and Gln666; see above), we conclude that the intra-subunit interface residues are crucial as they may form a pivot (see circled region in Fig. S3) to modulate the FMN domain motions during the IET process. According to the principle of microscopic reversibility, the reaction pathway for the reverse reaction is the exact opposite of the pathway for the forward reaction. Therefore, this pivot might be required to form a key

intermediate state on the reverse pathway when the FMN domain approaches to the heme domain from a large number of free states. The formation of such an intermediate presumably reduces the randomness of the FMN domain motions, and augments the electron transfer process.

3.3. The role of CaM in the motion of the FMN domain

In the post-IET state, the heme A-CaM interactions (Fig. 9b) are similar to that of the pre-IET state. Backbone oxygen of heme A domain residue Arg452 still forms a hydrogen bond with CaM residue Asp95. Two pairs of salt bridges between heme A domain residues Arg83, Arg86 and CaM residues Glu119, Asp122 are kept intact. In addition, heme A residues Gln97 and Thr95 loosely interact with CaM residues Gln135 and Ser101, respectively, through hydrogen bonds.

On the other hand, interactions between heme B domain and CaM in the post-IET state (Fig. 9c) are notably different from that in the pre-IET state. Heme B domain residues, Glu285, Asp 292 and Lys497, which do not interact with CaM in the pre-IET state, now form salt bridges with CaM residues Arg106, Lys115 and Asp118, respectively. In addition, the heme B coil residue Asp274 forms a strong salt bridge with CaM residue Arg37. The heme B domain linker residues Arg510 and Arg511 also form salt bridges with CaM residues Glu120 and Glu114, respectively. These interactions together appear to pull CaM closer to the heme B domain, indicated by a shorter distance between the linker residues Gln502 and Arg511 after the IET: the distance between two $\text{C}\alpha$ atoms of Gln502 and Arg511 changes from ~19 Å before the IET to ~15 Å after the IET. This motion likely facilitates the departure of the FMN domain from the heme A domain after the IET.

To better illustrate the details of the conformational changes in CaM with respect to heme B domain, the heme domains in the conformations at 60 ns of the oxyFMN construct in the pre- and post-IET states are superimposed in Fig. 10a. By looking into the changes in the CaM-interacting FMN domain residues, one can conclude that the conformational changes in CaM may directly affect the motion of the FMN domain. After the IET the first residue of the CaM-binding helix (Leu515) is shifted by about 2 Å, while Ser535 (the end of the helix) is shifted by about 14 Å (Fig. 10b). The movement of CaM is thus accompanied with its rotation around the CaM-binding helix Leu515–Ser535. The

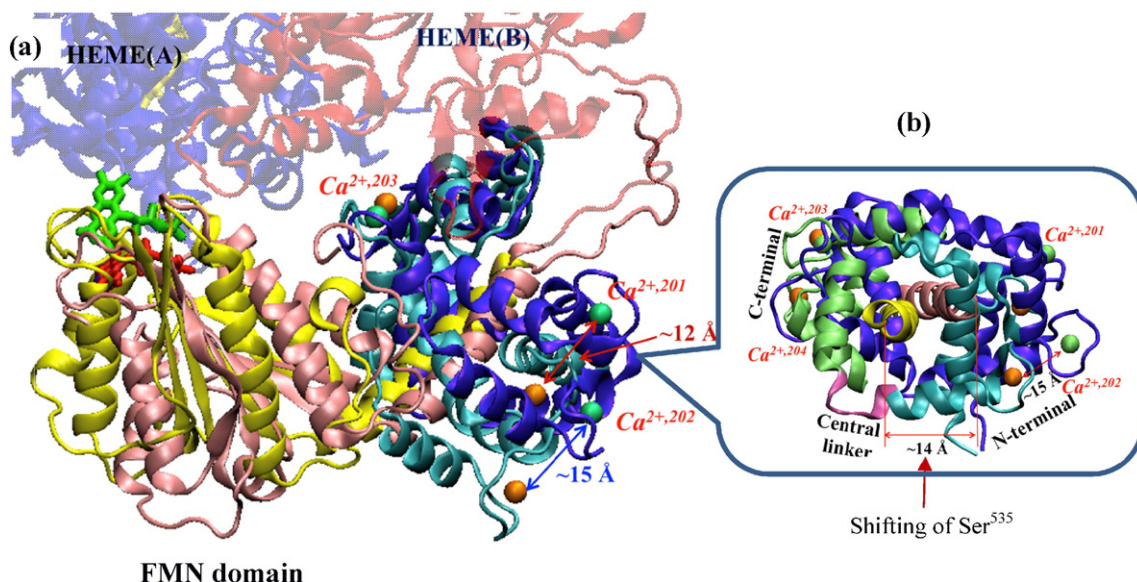


Fig. 10. (a) The heme domains in two conformations at 60 ns of human iNOS oxyFMN-CaM in the pre- and post-IET states are superimposed to illustrate the motions of the FMN domain (colored in yellow and pink for the pre- and post-IET states, respectively) and CaM (pre-IET: cyan; post-IET: purple). (b) CaM in the post-IET state (violet) and the pre-IET state (cyan: N-terminal, green: C-terminal, mauve: central linker); the CaM-binding helix of NOS in the pre- and post-IET states is colored yellow and bazaar, respectively. Calcium ions are shown in spheres and labeled.

rotation dismisses the interaction between the CaM and heme A domain (Fig. 9) that exist in the pre-IET state, and establishes new interactions between heme B domain residues (Glu285, Asp292, Lys497) and CaM residues (Arg106, Lys115, Asp118). This leads to the new interactions between C-lobe of CaM and N-terminal of the heme B domain after the IET (Fig. 9b). These CaM residues, along with the aforementioned intra-subunit pivot (FMN domain residues Glu661–Glu666 and heme B residues His404–Leu406; Fig. S3), may restrain the overall conformational freedom of the FMN domain in the post-IET state.

The positions of two bound Ca^{2+} ions (labeled as 201 and 202 in Fig. 10) move by ~ 15 and $\sim 12 \text{ \AA}$, respectively, between the pre- and post-IET states. The other two Ca^{2+} ions (203, 204), which locate near the CaM/heme B domain interface, only move by about 5 \AA and 2 \AA , respectively. This indicates that the N-terminal of the CaM protein has a larger conformational movement during the FMN–heme IET than the C-terminal. This is expected since the CaM C-terminal interacts with the NOS heme B domain, resulting in less motion freedom.

3.4. Steered molecular dynamics simulation

The oxyFMN·CaM conformations in the post-IET state are constrained with $\text{Fe}\cdots\text{N}_5$ distance shorter than 31 \AA in the 60 ns MD simulations (Fig. 4). It is interesting to investigate whether there is a bottleneck preventing the FMN domain from being totally free of binding to heme domain. We thus carried out a constant speed steered molecular dynamics (SMD) simulation to further separate the FMN and heme domains. Briefly, to pull the FMN domain away from the heme domain, a force was applied on the FMN domain in the direction from the heme A domain Fe to the FMN domain center. The pulling speed is set as $5 \text{ \AA}/\text{ns}$, with a spring constant of $5.0 \text{ kcal/mol}\cdot\text{\AA}^2$. The $\text{Fe}\cdots\text{N}_5$ (FMN) distance was pulled from $\sim 22 \text{ \AA}$ to $\sim 48 \text{ \AA}$ during the SMD simulation (Fig. 11). Analysis of the SMD data indicated how inter-domain interactions between the heme and FMN domains are gradually lost when these two domains are separated further.

Fig. 11 shows a plot of force versus the $\text{Fe}\cdots\text{N}_5$ (FMN) distance in the SMD process. There are two force peaks before 35 \AA . The first peak at $\sim 24 \text{ \AA}$ is related to the interdomain FMN/heme interactions when the FMN domain is docked on the heme domain. The key interactions are similar to the MD simulation above. Specifically this includes the aforementioned inter-subunit interactions of the FMN domain with the heme domain, and intra-subunit interactions in the pivot region. When the FMN domain is pulled away from the heme center to the second peak at $\sim 27 \text{ \AA}$, the inter-subunit interactions disappear, while the pivot remains intact. The pulling force also causes the FMN domain to swing around the pivot, instead of translating away from the heme domain, where the inter-domain interactions located afar from the pivot are disrupted first. When pulled further apart, the pivot structure is disrupted and eventually broken when the $\text{Fe}\cdots\text{N}_5$ (FMN) distance reaches beyond 35 \AA .

Our SMD results thus indicated the existence of a pivot region that correlates with the bottleneck. This prevents the FMN domain from becoming completely free of binding to the heme domains. To validate the

finding, we carried out a MD simulation on a conformation with the $\text{Fe}\cdots\text{N}_5$ (FMN) distance at around 35 \AA . As one can see from Fig. S4, the $\text{Fe}\cdots\text{N}_5$ (FMN) distance quickly reaches 40 \AA after 3 ns, where the FMN domain is free and the pivot no longer exists. This indicates that once it passes or comes very close to the bottleneck, the FMN domain can readily move toward completely free of binding to the heme domains.

Recent FMN fluorescence lifetime studies on iNOS [19], nNOS [18] and eNOS [56] proteins revealed a series of NOS conformations. Their results indicated that enablement of the conformational cycle by CaM binding is an important paradigm for control in nNOS [18]. We have shown that NOS exists in an equilibrium of open and docked conformations with a continuum of free (undocked) conformations [21]. Interestingly, cryo-EM studies of the three NOS isoforms [23–26] confirmed the shuttling motion of the FMN domain, and found a range of conformations enabled by the flexible tethers. These conformations reveal that CaM activates NOS by binding to the CaM-binding linker (which constrains rotational motions of the reductase domain relative to the heme domain [24]) and by directly binding to the heme domain [23]. In line with the cryo-EM studies, a pulsed EPR study confirmed that CaM binding induces a shift in the conformational equilibrium to drive electron transfer across the NOS domains ($\text{NADPH} \rightarrow \text{FAD} \rightarrow \text{FMN} \rightarrow \text{heme}$) [22]. Our MD simulation results are in line with these experimental findings. Moreover, the interactions of the residues identified in our work, especially those of the pivot, are proposed to allow the FMN domain to recognize the output state out of a multi-dimensional conformational space. Specifically, when in the output state, the FMN can move toward the heme domain with an appropriate degree of freedom, and eventually dock at proper positions, resulting in efficient IET and NO production.

There is strong experimental evidence that in addition to the long range shuttling motion between the FAD and heme domains, the FMN domain at the heme domain undergoes short-range sampling motions to productively dock onto the heme domain [55,57]. This short-range search for the optimal docking position is referred to as conformational sampling and is in part guided by complementary charged residues on the domain-domain FMN–heme interface [37,55]. These conformational changes enable efficient FMN–heme IET in the output state. Our computational simulation results support the conformational sampling model, in which sampling of a continuum of conformational states gives a range of transient donor–acceptor complexes, only a subset of which are IET-competent [16,18,58]. This presents an important mechanism for regulation in NOS enzyme, which avoids the necessity for tight binding of the FMN domain to achieve efficient IET.

This study used a bi-domain oxyFMN construct that consists of the oxygenase and FMN domains along with the CaM-binding linker. This construct was originally designed to favor observation of the NOS output state by precluding FAD/FMN interactions and favoring interactions between the FMN-binding domain and the oxygenase domain [31]. Biochemical and kinetic studies have demonstrated that it is a valid model of the NOS output state [4,5]. One can argue that the results obtained from the bi-domain oxyFMN system may not be fully applicable to holo-NOS. However, utilization of a similar bi-domain construct of P450 BM3 yielded results that were helpful in understanding the full-length enzyme mechanism [59,60]. Since the interdomain FMN/heme contacts are specific [61], the docked IET complex structure should be similar in the oxyFMN and full-length NOS. Indeed, the output state complex models [43] were fit without any alteration into the EM density of full-length iNOS protein [23]. The results for the docking complex structure obtained for the oxyFMN construct should therefore be generally applicable to the full-length NOS.

The FMN domain shuttling mechanism (Fig. 1) also operates in the ancestral electron transfer systems (e.g., flavodoxin/flavodoxin reductase), while the novel aspect of the NOS enzyme is the involvement of CaM. The CaM-binding linker in iNOS binds CaM at a basal level of Ca^{2+} , while in nNOS and eNOS the CaM binding requires an increase in intracellular $[\text{Ca}^{2+}]$ [1,62]. CaM activates NO synthesis through two

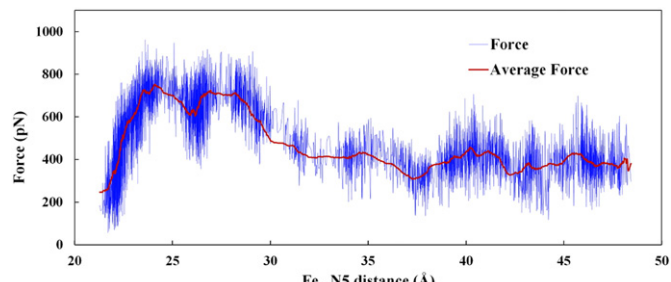


Fig. 11. Force profile from the SMD simulation when the FMN domain is further pulled away from heme A domain.

mechanisms. The first mechanism is unique to eNOS and nNOS, where the CaM binding releases the FMN domain from its interaction with the FAD/NADPH domain, allowing the FMN domain to transfer electrons to acceptors such as cytochrome *c*. This is a necessary but not a sufficient condition for NO production by eNOS/nNOS, which requires additional CaM-dependent promotion of the heme/FMN domain interactions (this second function of CaM is involved in formation of the output state of all the three NOS isoforms [5]). The docked FMN/heme state structures of the three NOS isoforms should be similar because the charged surface residues at the docking FMN/heme interface are highly conserved among the isoforms [37,38,53,55]. On the other hand, the conformational distributions in the CaM-bound NOS isoforms differ distinctly, with eNOS having the least docked state percentile, and iNOS having the highest docked state population, as suggested by the recent cryo-EM data showing more blurred images of nNOS and eNOS [23]. The main difference between eNOS/nNOS and iNOS is in CaM-responsive control elements, including an autoregulatory (AR) insert within the FMN domain of eNOS/nNOS [63], which does not exist in iNOS, and a C-terminal tail (CT), which differs in length among the three isoforms [64]. Mounting evidence shows that the AR insert exerts its regulatory function not only by competing with CaM binding [62], but also by stabilizing certain NOS states. In the absence of CaM, the AR insert and CT lock the FMN domain to its reductase complex [65]. When CaM binds at high $[Ca^{2+}]$, the insert is displaced so that the FMN domain is released and is able to shuttle electrons between the FAD and heme domains. Furthermore, recent studies by Masters [66] and us [11,67] show that the AR insert is also involved in stabilizing the docked FMN/heme state. Despite a wealth of available kinetics data, the underlying structural mechanism by which the AR insert and CT are involved in interactions between the FMN and heme domains remains elusive. It is thus interesting to conduct comparative computational and experimental studies of the oxyFMN constructs and holoenzymes of the three NOS isoforms, in order to better understand the molecular underpinning of CaM control of the electron transfer and NO production.

4. Conclusions

Emerging evidence showed that the CaM-controlled docking between the NOS FMN and heme domains is highly dynamic, but the underlying molecular mechanism is unclear. In this work, we have conducted molecular dynamics simulations on a human iNOS oxyFMN·CaM construct in both the $[Fe(III)][FMNH^-]$ and $[Fe(II)][FMNH^+]$ oxidation states. To the best of our knowledge, we provided the first computational evidence supporting the departure of FMN domain from heme center after the IET. In other words, the conformational change required for efficient IET is redox-dependent. Interestingly, redox-dependent domain movements have been demonstrated in the catalytic cycle of homologous P450 reductase [68], in which the tethered shuttle model also operates in the ancestral electron transfer system.

The computational results revealed a plausible mechanism of the FMN domain motions, as well as the mechanism by which CaM regulates the docking of the FMN domain to the heme active site. Our simulations identified specific residues on the heme, FMN and CaM domains important in optimal docking of the FMN domain to the heme domain. The predictions of the key interacting sites are well supported by experimental data in the literature. These dynamic interactions ensure that the FMN domain moves with appropriate degrees of freedom and docks to proper positions at the ends, resulting in efficient IET and NO production. The control of FMN domain motion by these specific interactions is important for NOS function since it facilitates directional electron transfer across the protein by appropriately modifying the conformational space available for the NOS protein. This work should inspire and guide future experiments to determine new specific sites involved in the electron transfer in NOS.

Abbreviations

NO	nitric oxide
NOS	nitric oxide synthase
CaM	calmodulin
eNOS	endothelial NOS
nNOS	neuronal NOS
iNOS	inducible NOS
NOSOxy	oxygenase domain of NOS
oxyFMN	bi-domain NOS construct in which only the oxygenase and FMN domains along with the CaM-binding region are present
FMNH ⁺	FMN semiquinone
FMN _{hq}	FMN hydroquinone
H ₄ B	(6R)-5,6,7,8-tetrahydrobiopterin
IET	interdomain electron transfer
MD	molecular dynamics
rmsd	root-mean-square deviations
EM	electron microscopy
SMD	steered molecular dynamics

Acknowledgments

This work was supported by grants to Y.S. from Florida Gulf Coast University ORSP (28147-ORG400100) and C.F. from the National Institutes of Health (GM081811), the National Science Foundation (CHE-1150644) and AHA grant-in-aid (12GRNT11780019).

Appendix A. Supplementary data

The topologies of ferrous heme, ferric heme, semiquinone and hydroquinone forms of FMN, and H₄B; the trajectories of the Fe···N₅ (FMN) distance from other molecular dynamics simulations; a figure showing the pivot region. Supplementary data to this article can be found online at <http://dx.doi.org/10.1016/j.jinorgbio.2015.08.006>.

References

- [1] W.K. Alderton, C.E. Cooper, R.G. Knowles, Biochem. J. 357 (2001) 593–615.
- [2] U. Förstermann, W.C. Sessa, Eur. Heart J. 33 (2012) 829–837.
- [3] R.A. Serafini, M.C. Primi, G.H. Trossini, E.I. Ferreira, Curr. Med. Chem. 19 (2012) 386–405.
- [4] C. Feng, L. Chen, W. Li, B.O. Elmore, W. Fan, X. Sun, J. Inorg. Biochem. 130 (2014) 130–140.
- [5] C. Feng, Coord. Chem. Rev. 256 (2012) 393–411.
- [6] K. Panda, S. Ghosh, D.J. Stuehr, J. Biol. Chem. 276 (2001) 23349–23356.
- [7] C.J. Feng, G. Tollin, M.A. Holliday, C. Thomas, J.C. Salerno, J.H. Enemark, D.K. Ghosh, Biochemistry 45 (2006) 6354–6362.
- [8] C.J. Feng, C. Thomas, M.A. Holliday, G. Tollin, J.C. Salerno, D.K. Ghosh, J.H. Enemark, J. Am. Chem. Soc. 128 (2006) 3808–3811.
- [9] C.J. Feng, G. Tollin, J.T. Hazzard, N.J. Nahm, J.G. Guillemette, J.C. Salerno, D.K. Ghosh, J. Am. Chem. Soc. 129 (2007) 5621–5629.
- [10] M.M. Haque, K. Panda, J. Tejero, K.S. Aulak, M.A. Fadlalla, A.T. Mustovich, D.J. Stuehr, Proc. Natl. Acad. Sci. U. S. A. 104 (2007) 9254–9259.
- [11] C.J. Feng, L.J. Roman, J.T. Hazzard, D.K. Ghosh, G. Tollin, B.S.S. Masters, FEBS Lett. 582 (2008) 2768–2772.
- [12] H. Li, A. Das, H. Sibhatu, J. Jamal, S.G. Sligar, T.L. Poulos, J. Biol. Chem. 283 (2008) 34762–34772.
- [13] R.P. Ilagan, M. Tiso, D.W. Konas, C. Hemann, D. Durra, R. Hille, D.J. Stuehr, J. Biol. Chem. 283 (2008) 19603–19615.
- [14] A. Welland, P.E. Garnaud, M. Kitamura, C.S. Miles, S. Daff, Biochemistry 47 (2008) 9771–9780.
- [15] C.J. Feng, A. Dupont, N. Nahm, D. Spratt, J.T. Hazzard, J. Weinberg, J. Guillemette, G. Tollin, D.K. Ghosh, J. Biol. Inorg. Chem. 14 (2009) 133–142.
- [16] R.P. Ilagan, J.S. Tejero, K.S. Aulak, S.S. Ray, C. Hemann, Z.-Q. Wang, M. Gangoda, J.L. Zweier, D.J. Stuehr, Biochemistry 48 (2009) 3864–3876.
- [17] R. Sanae, F. Kurokawa, M. Oda, S. Ishijima, I. Sagami, Biochemistry 50 (2011) 1714–1722.
- [18] J.C. Salerno, K. Ray, T. Poulos, H. Li, D.K. Ghosh, FEBS Lett. 587 (2013) 44–47.
- [19] D.K. Ghosh, K. Ray, A.J. Rogers, N.J. Nahm, J.C. Salerno, FEBS J. 279 (2012) 1306–1317.
- [20] M. Piazza, J.G. Guillemette, T. Dieckmann, Biochemistry 54 (2015) 1989–2000.
- [21] A.V. Astashkin, L. Chen, X. Zhou, H. Li, T.L. Poulos, K.J. Liu, J.G. Guillemette, C. Feng, J. Phys. Chem. A 118 (2014) 6864–6872.
- [22] A. Sobolewska-Stawiarz, N.G.H. Leferink, K. Fisher, D.J. Heyes, S. Hay, S.E.J. Rigby, N.S. Scrutton, J. Biol. Chem. 289 (2014) 11725–11738.

[23] M.G. Campbell, B.C. Smith, C.S. Potter, B. Carragher, M.A. Marletta, Proc. Natl. Acad. Sci. U. S. A. 111 (2014) E3614–E3623.

[24] N. Volkmann, P. Martásek, L.J. Roman, X.-P. Xu, C. Page, M. Swift, D. Hanein, B.S. Masters, J. Struct. Biol. 188 (2014) 46–54.

[25] A.L. Yokom, Y. Morishima, M. Lau, M. Su, A. Glukhova, Y. Osawa, D.R. Southworth, J. Biol. Chem. 289 (2014) 16855–16865.

[26] A. Persechini, Q.K. Tran, D.J. Black, E.P. Gogol, FEBS Lett. 587 (2013) 297–301.

[27] M. Piazza, V. Taiakina, S.R. Guillemette, T. Dieckmann, Biochemistry 53 (2014) 1241–1249.

[28] M. Piazza, K. Futrega, D.E. Spratt, T. Dieckmann, J.G. Guillemette, Biochemistry 51 (2012) 3651–3661.

[29] M.M. Haque, C. Kenney, J. Tejero, D.J. Stuehr, FEBS J. 278 (2011) 4055–4069.

[30] M.M. Haque, M. Bayachou, J. Tejero, C. Kenney, N.M. Pearl, S.-C. Im, L. Waskell, D.J. Stuehr, FEBS J. 281 (2014) 5325–5340.

[31] D.K. Ghosh, M.A. Holliday, C. Thomas, J.B. Weinberg, S.M.E. Smith, J.C. Salerno, J. Biol. Chem. 281 (2006) 14173–14183.

[32] H.Y. Li, C.S. Raman, C.B. Glaser, E. Blasko, T.A. Young, J.F. Parkinson, M. Whitlow, T.L. Poulos, J. Biol. Chem. 274 (1999) 21276–21284.

[33] C. Xia, I. Misra, T. Iyanagi, J.-J.P. Kim, J. Biol. Chem. 284 (2009) 30708–30717.

[34] B.G. Pierce, Y. Hourai, Z. Weng, PLoS ONE 6 (2011) e24657.

[35] R. Chen, L. Li, Z. Weng, Proteins Struct. Funct. Genet. 52 (2003) 80–87.

[36] M.M. Haque, M. Bayachou, M.A. Fadlalla, D. Durra, D.J. Stuehr, Biochem. J. 450 (2013) 607–617.

[37] J. Tejero, L. Hannibal, A. Mustovich, D.J. Stuehr, J. Biol. Chem. 285 (2010) 27232–27240.

[38] K. Panda, M.M. Haque, E.D. Garcin-Hosfield, D. Durra, E.D. Getzoff, D.J. Stuehr, J. Biol. Chem. 281 (2006) 36819–36827.

[39] M.M. Haque, M. Fadlalla, Z.Q. Wang, S.S. Ray, K. Panda, D.J. Stuehr, J. Biol. Chem. 284 (2009) 19237–19247.

[40] A.V. Astashkin, B.O. Elmore, W. Fan, J.G. Guillemette, C. Feng, J. Am. Chem. Soc. 132 (2010) 12059–12067.

[41] J.C. Phillips, R. Braun, W. Wang, J. Gumbart, E. Tajkhorshid, E. Villa, C. Chipot, R.D. Skeel, L. Kalé, K. Schulten, J. Comput. Chem. 26 (2005) 1781–1802.

[42] A.D. MacKerell, D. Bashford, Bellott, R.L. Dunbrack, J.D. Evanseck, M.J. Field, S. Fischer, J. Gao, H. Guo, S. Ha, D. Joseph-McCarthy, L. Kuchnir, K. Kuczera, F.T.K. Lau, C. Mattos, S. Michnick, T. Ngo, D.T. Nguyen, B. Prodhom, W.E. Reiher, B. Roux, M. Schlenkrich, J.C. Smith, R. Stote, J. Straub, M. Watanabe, J. Wiórkiewicz-Kuczera, D. Yin, M. Karplus, J. Phys. Chem. B 102 (1998) 3586–3616.

[43] B.C. Smith, E.S. Underbakke, D.W. Kulp, W.R. Schief, M.A. Marletta, Proc. Natl. Acad. Sci. U. S. A. 110 (2013) E3577–E3586.

[44] A. Altun, W. Thiel, J. Phys. Chem. B 109 (2005) 1268–1280.

[45] P.J. Hay, W.R. Wadt, J. Chem. Phys. (1985) 299–310.

[46] C.M. Bathelt, J. Zurek, A.J. Mulholland, J.N. Harvey, J. Am. Chem. Soc. 127 (2005) 12900–12908.

[47] D. Fishelovitch, S. Shaik, H.J. Wolfson, R. Nussinov, J. Phys. Chem. B 114 (2010) 5964–5970.

[48] F. Autenrieth, E. Tajkhorshid, J. Baudry, Z. Luthey-Schulten, J. Comput. Chem. 25 (2004) 1613–1622.

[49] P.L. Freddolino, M. Dittrich, K. Schulten, Biophys. J. 91 (2006) 3630–3639.

[50] D. Fishelovitch, C. Hazan, S. Shaik, H.J. Wolfson, R. Nussinov, J. Am. Chem. Soc. 129 (2007) 1602–1611.

[51] W.L. Jorgensen, J. Chandrasekhar, J.D. Madura, R.W. Impey, M.L. Klein, J. Chem. Phys. 79 (1983) 926–935.

[52] C.C. Page, C.C. Moser, X.X. Chen, P.L. Dutton, Nature 402 (1999) 47–52.

[53] J. Sempombe, B.O. Elmore, X. Sun, A. Dupont, D.K. Ghosh, J.G. Guillemette, M.L. Kirk, C. Feng, J. Am. Chem. Soc. 131 (2009) 6940–6941.

[54] J. Sempombe, M.G.I. Galinato, B.O. Elmore, W. Fan, J.G. Guillemette, N. Lehnert, M.L. Kirk, C. Feng, Inorg. Chem. 50 (2011) 6859–6861.

[55] W. Li, L. Chen, C. Lu, B.O. Elmore, A.V. Astashkin, D.L. Rousseau, S.-R. Yeh, C. Feng, Inorg. Chem. 52 (2013) 4795–4801.

[56] D.C. Arnett, A. Persechini, Q.-K. Tran, D.J. Black, C.K. Johnson, FEBS Lett. 589 (2015) 1173–1178.

[57] W. Li, L. Chen, W. Fan, C. Feng, FEBS Lett. 586 (2012) 159–162.

[58] D. Leys, N.S. Scrutton, Curr. Opin. Struct. Biol. 14 (2004) 642–647.

[59] I.F. Seviroukova, H. Li, H. Zhang, J.A. Peterson, T.L. Poulos, Proc. Natl. Acad. Sci. U. S. A. 96 (1999) 1863–1868.

[60] I.F. Seviroukova, J.T. Hazzard, G. Tollin, T.L. Poulos, J. Biol. Chem. 274 (1999) 36097–36106.

[61] L.J. Roman, J. McLain, B.S.S. Masters, J. Biol. Chem. 278 (2003) 25700–25707.

[62] L.J. Roman, P. Martasek, B.S.S. Masters, Chem. Rev. 102 (2002) 1179–1189.

[63] J.C. Salerno, D.E. Harris, K. Irizarry, B. Patel, A.J. Morales, S.M.E. Smith, P. Martasek, L.J. Roman, B.S.S. Masters, C.L. Jones, B.A. Weissman, P. Lane, Q. Liu, S.S. Gross, J. Biol. Chem. 272 (1997) 29769–29777.

[64] L.J. Roman, P. Martasek, R.T. Miller, D.E. Harris, M.A. de la Garza, T.M. Shea, J.J.P. Kim, B.S.S. Masters, J. Biol. Chem. 275 (2000) 29225–29232.

[65] E.D. Garcin, C.M. Bruns, S.J. Lloyd, D.J. Hosfield, M. Tiso, R. Gachhui, D.J. Stuehr, J.A. Tainer, E.D. Getzoff, J. Biol. Chem. 279 (2004) 37918–37927.

[66] L.J. Roman, B.S.S. Masters, J. Biol. Chem. 281 (2006) 23111–23118.

[67] S.P. Panda, W. Li, P. Venkatakrishnan, L. Chen, A.V. Astashkin, B.S.S. Masters, C. Feng, L.J. Roman, FEBS Lett. 587 (2013) 3973–3978.

[68] W.-C. Huang, J. Ellis, Peter C.E. Moody, Emma L. Raven, Gordon C.K. Roberts, Structure 21 (2013) 1581–1589.